Drug Design, Development and Therapy

Dovepress
Taylor & Francis Group

Open Access Full Text Article

ORIGINAL RESEARCH

SRN-901, a Novel Longevity Drug, Extends Lifespan and Healthspan by Targeting Multiple Aging Pathways

Brett Weiss[1], Daniel R Miranda[1], Dylan Arrazati[1], Rui Cao[1], Jiaqi Chen[2,3], Yongzheng Liu[3,4], David Brown[1], George Marshall[1]

[1]Seragon Biosciences, Irvine, CA, USA; [2]School of Biomedical Engineering, Tsinghua University, Beijing, People's Republic of China; [3]Sinopharm-Seragon Biosciences, Beijing, People's Republic of China; [4]School of Medicine, Tsinghua University, Beijing, People's Republic of China

Correspondence: Brett Weiss; George Marshall, Seragon Biosciences, Irvine, CA, USA, Email bweiss@seragon.com; gmarshall@seragon.com

Introduction: Developing interventions to delay aging and improve lifespan and healthspan is a critical goal in aging research. Individual geroprotective compounds fail to address the complexity, interconnectedness, and dynamic nature of biological systems, limiting success in significantly extending lifespan and improving health. This study investigates the effects of SRN-901—a novel oral combinatorial drug that consists of urolithin A, quercetin, nicotinamide riboside, alpha-lipoic acid, and Seragon's SRN-820—on lifespan extension, frailty reduction, disease-related gene expression pathways, metabolic aging, and the proteome in 18-month-old mice fed a Western diet.

Results: SRN-901-treated mice showed a significant increase of 33% in median remaining lifespan compared to placebo-treated mice. Cox proportional hazards analysis revealed a hazard ratio of 0.54, indicating that SRN-901 treatment was associated with a 46% reduction in the hazard of death. While rapamycin increased lifespan in adult mice, nicotinamide mononucleotide (NMN), and nicotinamide riboside (NR) did not show significant differences in median lifespan compared to placebo. SRN-901 protected mice against increased frailty during aging, with baseline-normalized scores rising to 1.17 in treated mice and 1.57 in controls, corresponding to a 70% attenuation of frailty progression between pre-treatment (D-14) and post-treatment (D128; $p < 0.001$). Transcriptomic analyses revealed that SRN-901 modulates gene expression across pathways implicated in aging biology, including inflammation, apoptosis, and DNA repair, as well as gene sets associated with neurodegenerative disorders, including Alzheimer's disease. Metabolic profiling revealed that SRN-901 was associated with attenuation of several age-related metabolic shifts, resulting in a blood metabolite profile that more closely resembled that of younger mice. The upregulation of glutathione metabolism and other longevity-related pathways underscores SRN-901's role in enhancing cellular defenses against oxidative stress and maintaining metabolic health.

Discussion: These results highlight SRN-901 as a promising multi-compound candidate for extending lifespan and healthspan by targeting multiple aging pathways.

Keywords: SRN-901, mTOR, autophagy, mitophagy, senolytics, NAD+, lifespan, healthspan, longevity

Introduction

Aging is a complex biological process associated with declining physiological functions, increased frailty, susceptibility to cardiometabolic and neurodegenerative disorders, and increased mortality. The aging population has become a significant global issue, requiring efficient, large-scale measures to mitigate late-life ailments and improve human healthspan.[1,2] Among the prospective strategies, anti-aging pharmacotherapy is distinguished by its adaptability, controllability, and practicality, rendering it a compelling strategy for creating geroprotective interventions.[3]

Substantial progress has been achieved in the identification of substances possessing anti-aging properties. The DrugAge database catalogs more than 4000 lifespan experiments, including 372 conducted in *Mus musculus*.[4] In parallel, over 300 human genes and more than 2000 model organism genes have been implicated in aging and lifespan regulation[5]

https://doi.org/10.2147/DDDT.S594895
Received: 21 January 2026
Accepted: 20 March 2026
Published: 15 April 2026

offering an extensive pool of potential targets for drug development.[6] These single-target approaches often fail to address the systems-level complexity and interconnected nature of aging.[7]

To improve the efficacy of anti-aging therapies, attention has shifted toward developing and combining compounds that target many pathways simultaneously.[8] This strategy holds the potential for synergistic effects, wherein the combined impact of the compounds is greater than the sum of their individual effects. Key considerations for designing such combinations include minimizing off-target effects, avoiding cumulative toxicity, and ensuring that absorption is comparable to individual compounds.[9] The success of combination therapies in treating various diseases, such as type 2 diabetes, cancer, obesity, and hypertension, provides a strong foundation for applying this approach to aging-related interventions,[10] and databases documenting drug interactions and therapeutic outcomes further facilitate this research.[11] Nevertheless, studies specifically focused on combination therapies for lifespan extension remain scarce and fragmented.[12]

In this study, we investigated whether a combinatorial intervention could extend lifespan and improve healthspan in aged mice. Eighteen-month-old C57BL/6 mice were treated until death with SRN-901 (500 mg/kg/day), a novel oral formulation composed of a PI3K/Akt/mTOR pathway modulator, an autophagy-enhancing compound, an anti-inflammatory flavonoid, and an NAD^+ precursor. Frailty assessments were conducted before and after dosing, and blood samples were collected for transcriptomic and metabolomic analyses to evaluate molecular correlates of longevity.

Materials and Methods

Mice, Husbandry, and Diet Preparation

A total of 160 C57BL/6 mice (80 male and 80 pup-naïve female) were purchased from Charles River Laboratories at the age of 15 months and aged in the animal facility (HD Biosciences, San Diego) until they reached 18 months. Eighteen months of age was selected to model late-life intervention. In C57BL/6 mice, 18–24 months corresponds to late-middle to early-old age and aligns approximately with late-middle-aged to older adult humans, depending on the conversion model used.[13] Aligning murine age with appropriate human life stages is critical when modeling age-dependent pathologies, including metabolic dysfunction, neurodegeneration, and cancer, to avoid artificial or mistimed disease phenotypes. Mice were housed in groups of three or four per cage under standard conditions, including a 12-hour light/dark cycle (lights on at 7:00 AM, ambient temperature of 22 ± 2°C, and relative humidity of 50 ± 10%. To simulate human dietary patterns, mice were fed the Total Western Diet (TWD), a high-fat diet (ENVIGO TD.110424; 45% kcal from fat, 35% from carbohydrates, and 20% from protein; energy density 4.7 kcal/g) ad libitum, with free access to water. Body weight and food intake were measured weekly to monitor health and dietary compliance (Supplementary Figure 1). SRN-901 (500 mg/kg/day) and control were fed through oral gavage 6 days a week. SRN-901 was obtained from Seragon Biosciences. The 500 mg/kg/day SRN-901 dose was selected by combining nicotinamide riboside, quercetin, urolithin A, and alpha-lipoic acid in equimolar concentrations, consistent with doses previously reported in the literature to be well tolerated and to influence metabolic or aging-related pathways, together with Seragon's SRN-820 at an internally established percentage that produced robust target engagement without gastrointestinal intolerance in prior exploratory studies. NMN (300mg/kg) and NR (300mg/kg) were purchased from Effepharm, and fed through oral gavage 6 days a week. Rapamycin was mixed in food with a concentration of 14.4 ppm. All groups (SRN-901, NMN, NR, Rapamycin, and Placebo), underwent an identical handling and gavage schedule (same frequency, time-of-day, and volume) by trained staff using a standardized procedure using either group-specific drug or vehicle (water) and no deviation events were recorded.

Sample sizes were selected based on effect sizes reported in late-life intervention studies and were intended to provide >80% power to detect a 20–30% difference in median lifespan at α=0.05. Formal power calculations were not performed prior to initiating the study because of variability across reported survival and attrition rates. To minimize bias, mice were randomized into groups (SRN-901 and Control: n=44 per group; Rapamycin, NMN, and NR: n=24 per group) using a computer-generated randomization protocol. To minimize the impact of social hierarchy and aggression, mice were housed without replacement as individuals died at older ages. In cases where fight wounds necessitated removal for

humane reasons, all mice in the affected cage were removed from the study to avoid biasing the population toward dominant or non-dominant individuals.

Mice were inspected daily for health and welfare. Animals deemed unlikely to survive for more than an additional 48 hours, based on a predefined symptom checklist, were euthanized for humane reasons. The date of euthanasia was recorded and used as the best estimate of the date of natural death for statistical purposes. For mice found dead during daily inspections, the date of death was recorded. At necropsy, tumors were identified and recorded to calculate tumor incidence in each group. The principal endpoint of the study was age at death (for mice found dead) or age at euthanasia (for mice euthanized due to severe morbidity). For Euthanasia, mice were exposed to 4% isoflurane. Animals were monitored closely, watching for cessation of motion including breathing. Death was confirmed by cervical dislocation under anesthesia which was performed. All animal studies were conducted by a licensed contract research organization (CRO) operating under institutional animal care and use committee (IACUC) oversight (HD Biosciences, San Diego CA). All procedures were performed in accordance with applicable national and institutional guidelines for the care and use of laboratory animals, including the Guide for the Care and Use of Laboratory Animals. The animals in this study were C57BL/6 mice and did not require a license/permit for third party research use.

Frailty Analysis

Frailty was assessed (Supplementary Figure 1) using a validated mouse clinical frailty index (FI) scoring system, as previously described.[14] The FI evaluates a range of health parameters to provide a quantitative measure of frailty, with higher scores indicating greater frailty. Assessments were conducted at two time points: 14 days before the initiation of dosing (baseline) and 128 days after dosing began.

The FI scoring system included 24 non-invasive health parameters, such as integumentary, physical, musculoskeletal, ocular, nasal, digestive, urogenital, and respiratory systems. Each parameter was scored on a scale of 0 (no deficit), 0.5 (mild deficit), or 1 (severe deficit). The total FI score was calculated as the sum of all deficits, with a maximum possible score of 24. Frailty index scores are presented as mean ± standard error of the mean (SEM). To account for any baseline imbalances, frailty scores were analyzed using a two-way repeated-measures ANOVA with group and time as factors, and post hoc comparisons were performed on change-from-baseline scores. A p-value of < 0.05 was considered statistically significant. Investigators performing frailty scoring and lifespan analysis were blinded to treatment allocation, and treatment preparation was handled by personnel not involved in data collection.

Transcriptome Analysis

Sampling and Sequencing

RNA sequencing was performed on n=24 mice per group to investigate transcriptome-wide changes across experimental groups. Total RNA was extracted using TRIzol Kit (Invitrogen, Carlsbad, CA), with rigorous quality control implemented at multiple stages. RNA purity was assessed via NanoDrop™ spectrophotometry (A260/A280 > 1.9; A260/A230 > 2.0), integrity verified by Agilent™ 5400 Bioanalyzer (RIN > 8.0), and genomic DNA contamination excluded through 1% agarose gel electrophoresis. Strand-specific RNA-seq libraries were constructed using the NEBNext® Ultra II™ Directional RNA Library Prep Kit (New England Biolabs), following polyadenylated mRNA enrichment with poly-T magnetic beads. Critical steps included fragmentation of mRNA (94°C for 8 min), first-strand cDNA synthesis with random hexamers, and second-strand synthesis using dUTP for strand orientation preservation. Final libraries (300–500 bp inserts) were prepared through end repair, A-tailing, adapter ligation, and dual-size selection with AMPure XP system (Beckman Coulter).

Libraries were quantified via Qubit™ 4.0 Fluorometer and qPCR (KAPA Library Quant Kit), with size distribution validated using Agilent High Sensitivity DNA Kit. Equimolar pooled libraries were sequenced on an Illumina NovaSeq 6000 platform (2×150 bp paired-end reads), generating ~20 million high-quality reads per sample (Q30 > 85%).

Raw Sequencing Data Underwent Stringent Preprocessing

Adapters and low-quality bases (Q-score < 25) were trimmed using Fastp v0.23.2 with a 4-bp sliding window,[15,16] followed by ribosomal RNA depletion via Ribodetector v3.0 in -rrna mode; SILVA database.[17] Post-filtering reads (92.4% retention rate) were aligned to the GRCm39 reference genome (Mus Musculus Genome Assembly GRCm39, n. d.) using STAR v2.7.10b[18] with splice-aware parameters (–sjdbOverhang 149; –alignIntronMax 80,000), achieving 89.3% mean alignment efficiency. BAM files were indexed with Samtools v1.15[19] and gene-level counts were generated using FeatureCounts v2.0.3[20] in reverse-stranded mode (-s 2) with multi-mapping reads proportionally assigned (–fraction).

Differential Expression Analysis

Differential expression analysis employed a dual-method approach: DESeq2 v1.38.3[21] and edgeR v3.40.2.[22] For DESeq2, a multifactorial design matrix (~0 + time:condition) was implemented to disentangle treatment and temporal effects, and dispersion estimates were validated via diagnostic plots. Low-count genes (baseMean <10) and Ensembl gene ID duplicates were resolved through expression averaging. Differentially expressed genes (DEGs) were defined by $|\log2FoldChange| > 1$ and Benjamini-Hochberg adjusted p-value < 0.05 across three comparisons: pan-group treatment effects and sex-stratified analyses.[23]

Functional Annotation and Pathway Analysis

To establish evolutionary conservation of aging-associated transcriptional signatures, candidate DEGs were cross-referenced with three curated longevity databases: GenAge[24] (build 21), SynergyAge (2023 release),[25] Aging Atlas (RRID:SCR_024793).[26] Enrichment analyses were systematically conducted using clusterProfiler v4.6.0[27] with optimized parameters: Ensembl-to-Entrez ID conversion via org.Mm.egdb, GO term redundancy reduction through ReviGO semantic clustering,[28] and Benjamini-Yekutieli FDR correction.[29] Gene Set Enrichment Analysis (GSEA) was executed using fgsea v1.24.0[30] against MSigDB Hallmark gene sets.[31] Significantly altered pathways were projected onto human orthologs using Reactome's Cross-Species Inference Engine, and the longevity-regulating pathway (KEGG mmu04211[32] was visualized via Pathview v1.38.0.[33]

Metabolome Analysis

Sampling and Chromatographic Separation

Frozen whole blood (SRN-901 and control; n=12 mice per group) was homogenized in ice-cold methanol/water (80:20, v/v) using a Bead Ruptor Elite homogenizer (Omni International) at 4°C, followed by centrifugation (15,000×g, 10 min, 4°C) to pellet insoluble debris. Supernatants were lyophilized and reconstituted in 100 µL acetonitrile/water (1:1) for analysis. To ensure analytical reproducibility, quality control (QC) samples were generated by pooling equal aliquots from all experimental samples and injected every 10 runs throughout the sequence.

Chromatographic separation was achieved using a Waters ACQUITY UPLC HSS T3 column (2.1×100 mm, 1.8 µm) maintained at 40°C, coupled to a TripleTOF 6600 mass spectrometer (SCIEX) equipped with DuoSpray™ ion source. The mobile phase comprised 0.1% (v/v) formic acid in water (A) and acetonitrile (B), with the following elution gradient: 0–1 min 2% B, 1–12 min linear increase to 98% B, 12–14 min isocratic hold, 14–14.1 min return to 2% B, and 14.1–16 min column re-equilibration. Mass spectrometric detection was performed in both positive (ESI+, 5.0 kV) and negative (ESI-, −4.0 kV) ionization modes with the following parameters: curtain gas 35 psi, ion source gas 1 (55 psi) and gas 2 (60 psi), source temperatures of 550°C (ESI+) and 450°C (ESI-), mass range m/z 50–1000 for MS1 and m/z 25–1000 for MS2 scans, and collision energy ramping from 10–40 eV(Multi- and Megavariate Data Analysis. Part I Basic Principles and Applications. Second Revised and Enlarged Edition | Request PDF, n.d.).

Data Preparation

Raw mass spectrometry data were converted to mzXML format using ProteoWizard MSConvert (v3.0)[34] and processed through XCMS (v3.18.0)[35] with optimized workflows: The peaks with missing rate >50% in each group of samples were filtered. Missing values were imputed via k-nearest neighbors (k=10),[36] followed by QC-driven support vector regression (SVR) normalization to mitigate batch effects.[37] Metabolite annotation integrated three complementary strategies: 1)

matching against an in-house library of 1200 authenticated standards; 2) cross-referencing with HMDB (v5.0)[38,39] and METLIN (2023) databases[40] in silico prediction using MS-FINDER (v4.2) with SIRIUS fragmentation scores >4.0. Final metabolite identifications required coefficient of variation (CV) <30% in QC replicates and MS/MS spectral similarity confidence level ≥2 (out of 4-tiered confidence scoring system).

Raw mass spectrometry data were processed using the MetaboAnalystR package (v6.0). Quality control (QC) measures were implemented to filter unreliable reads based on low repeatability within the QC sample group, as determined by the relative standard deviation (RSD = SD/mean), with a threshold of 25%. To further refine the dataset, an additional variance filter was applied based on the interquartile range, retaining the top 95% of variance-exhibiting metabolites while filtering out the top 5% of highly variable features.

Following quality filtering, data were normalized using the pooled QC sample group to correct for batch effects and technical variability. Normalization included log10 transformation to reduce skewness and autoscaling to ensure metabolite standardization across all samples. These steps were performed to enhance comparability by minimizing systemic bias resulting from differences in measurement scales. After log10 transformation and autoscaling, distributions of metabolite intensities were visually assessed using Q–Q plots and histograms. For downstream analysis, FDR-adjusted p-values < 0.05 were considered significant.

Differential Metabolite Analysis

Heatmap generation was conducted using all 24 mouse samples absolute mean subtraction, with values considered equivalent if their absolute mean difference was less than 0.3 units and distinct if the absolute mean difference exceeded 0.7 units. These cutoffs were determined based on autoscaled values to provide robust visualization of metabolic variations. Differentially expressed metabolites were subjected to pathway enrichment analysis using the MetaboAnalystR package (v6.0).

To further investigate metabolic shifts from pre-treatment to post-treatment in the control group and the treatment group, a hierarchical statistical framework was utilized to reinforce statistical validity. For intra-group hypothesis testing, normally distributed paired data was assessed via paired t-tests, while non-normal paired data was evaluated via Wilcoxon signed-rank test.[41] For inter-group hypothesis testing, independent *t*-test with Welch's correction[42] was implemented for normally distributed metabolic shifts to address potential heteroscedasticity, while Mann–Whitney *U*-test[43] was employed for nonparametric distributions. Differential metabolites were selected using an FDR threshold of $p < 0.05$.

Functional Annotation and Pathway Analysis

Annotated metabolites were mapped to their corresponding pathways in the Kyoto Encyclopedia of Genes and Genomes (KEGG) database to identify significantly altered metabolic networks. The hypergeometric test was employed to determine pathway significance, with p-values adjusted for multiple testing using the false discovery rate (FDR) method.

Pathways were ranked based on enrichment scores (-log10(p-value)), and pathway directionality was assessed using z-score calculations to distinguish upregulated and downregulated pathways. Visualization was performed using KEGG pathway heatmaps, bar plots, and enrichment graphs to highlight metabolic alterations induced by SRN-901 treatment. Pathways with FDR-adjusted p-values < 0.05 were considered significantly enriched and were used to infer SRN-901's impact on metabolic aging and longevity-associated processes.

Proteomics Analysis

Sampling and Data Acquisition

Freshly collected mouse serum samples were immediately snap-frozen in liquid nitrogen and stored at −80°C in low-protein-binding cryovials (Eppendorf Protein LoBind®) to minimize surface adsorption (n=24 per group). For proteomic processing, samples were thawed at 4°C under controlled conditions and subjected to automated handling using an SP100 liquid handling system (SPT Labtech) to ensure protocol consistency. Aliquots (50 µL) were transferred to a 96-well mPCR plate (Bio-Rad) for parallelized workflow execution. Protein enrichment was achieved through incubation with polymer core-silica shell magnetic nanoparticles (200 nm diameter, 1:10 v/v nanoparticle-to-sample ratio) under

optimized binding conditions (25°C, 800 rpm orbital shaking for 30 min), followed by three washes with low-salt buffer (50 mM ammonium bicarbonate, pH 8.0) to remove nonspecific binders. Captured proteins underwent sequential reduction (10 mM dithiothreitol, 56°C for 30 min) and alkylation (20 mM iodoacetamide, 25°C for 20 min in dark conditions), with on-bead digestion performed using sequencing-grade trypsin (Promega, 1:20 enzyme-to-substrate ratio) at 37°C for 16 h under continuous agitation (500 rpm). Resulting peptides were desalted using C18 StageTips (Thermo Scientific), eluted in 80% acetonitrile/0.1% formic acid, and quantified via UV absorbance at 280 nm (NanoDrop™) prior to vacuum drying.

Peptide and Protein Quantification

For LC-MS/MS analysis, lyophilized peptides were reconstituted in 0.1% formic acid and loaded onto a Vanquish Neo UHPLC system (Thermo Scientific) equipped with a 50 cm µPAC C18 column (PharmaFluidics). Chromatographic separation employed a 120-min gradient: 2–28% mobile phase B (0.1% formic acid in acetonitrile) over 90 min, 28–40% B over 10 min, 40–95% B over 5 min, followed by 15 min column re-equilibration at 500 nL/min. Mass spectrometric data were acquired on an Orbitrap Astral instrument (Thermo Scientific) operated in data-independent acquisition (DIA) mode with the following parameters: MS1 scans at 120,000 resolution (m/z 380–980), automatic gain control (AGC) target 300%; MS2 spectra collected via Astral analyzer with 3 m/z isolation windows and 15 normalized collision energy (NCE), achieving a 1.5 s MS1 cycle time coupled with 22 DIA windows.

Raw DIA files were processed using DIA-NN (v1.8.1)[44] in library-free mode against the UniProt Mus musculus proteome (2023-Q3 release) (Mus Musculus (Mouse) | Proteomes | UniProt, n.d.). Peptide-spectrum matches were filtered at 1% global false discovery rate (FDR) using a convolutional neural network classifier. Protein quantification via maxLFQ algorithm[45] incorporated delayed cross-run normalization with ComBat batch effect correction (sva R package v3.48.0),[46] while missing values (present in <50% samples) were imputed via k-nearest neighbors (k=5). Final abundances were scaled to the sample-wise median total intensity for inter-sample comparability.

Statistical Analysis

Proteomics data analysis employed a tiered statistical framework to ensure methodological robustness. For hypothesis testing, one-way ANOVA with Welch's correction[47] was implemented to accommodate potential heteroscedasticity across experimental groups, using log2-transformed intensity matrices for significance assessment. Fold-change calculations were derived from raw (non-log2) intensities to preserve absolute magnitude relationships. Multivariate exploration integrated principal component analysis (PCA) with mean-centered scaling and hierarchical clustering based on log2 (fold-change) transformed values, utilizing Euclidean distance metrics and the unweighted pair group method with arithmetic mean (UPGMA) algorithm for dendrogram construction.

Differential expression candidates were further refined through empirical Bayes moderated t-tests (limma R package v3.56.0)[48] with Benjamini-Hochberg false discovery rate (FDR) correction, applying stringent thresholds of $|\log2(\text{fold change})| > 1$ and FDR <0.05. Pathway enrichment analysis was conducted through dual complementary approaches: 1) Over-representation analysis using Fisher's exact test against the PathBank knowledgebase (2023-Q4 release),[49] encompassing metabolic, signaling, and disease-associated pathways; 2) Gene Ontology (GO)[50] and Reactome annotation via clusterProfiler (v4.6.0)[27] with q-value <0.1 and minimum 5-protein cluster size requirements.

Results

SRN-901 Administration in Adult Mice Extends Lifespan

To assess the efficacy of late-onset SRN-901 treatment, 18-month-old C57BL/6J mice were treated with SRN-901, placebo, or other anti-aging compounds, and mouse cohorts were followed until the predetermined humane endpoint to determine lifespan (Figure 1). During the treatment period, we did not notice a decline in body weight or food intake for either SRN-901-treated or placebo-treated mice across both sexes.

We found that SRN-901-treated mice (median: 350.5 days; 95% CI: 309.0–412.0; n = 38) showed a significant increase of 33% in median remaining lifespan compared to placebo-treated mice (median: 263.5 days; 95% CI: 241.0–305.0; n = 42; $p < 0.001$) (Figure 2 and Supplementary Table 1.1). Cox proportional hazards analysis revealed

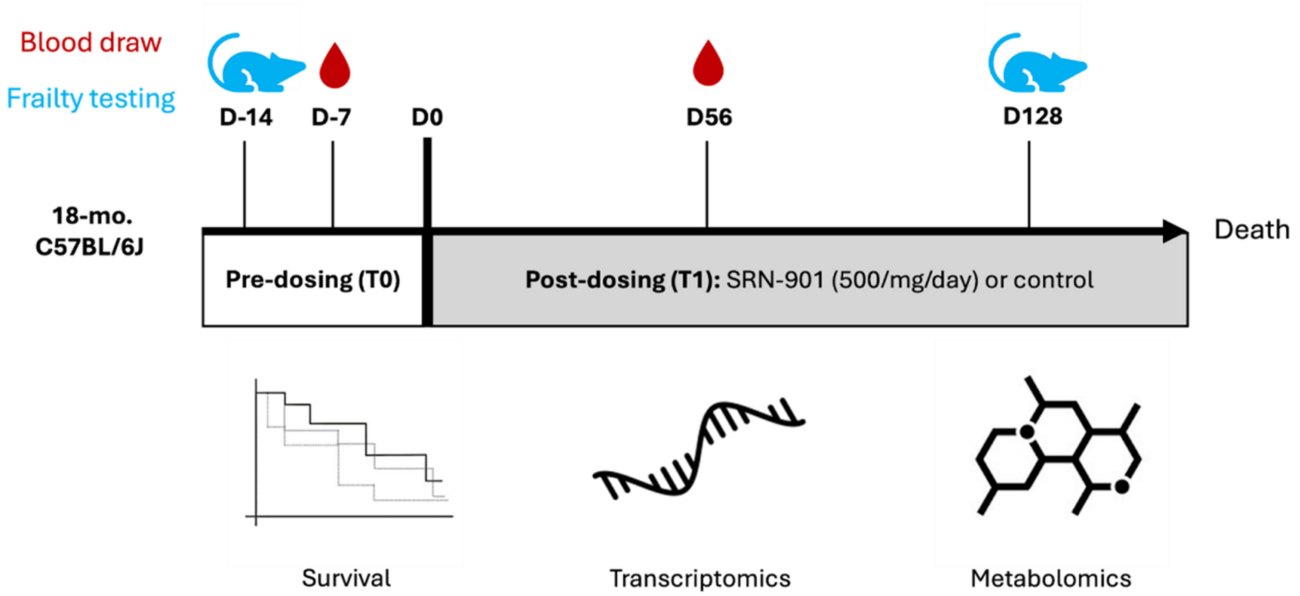

Figure 1 Experimental design for testing lifespan and healthspan effects of SRN-901 on adult mice. Experimental design and study workflow illustrating animal age, randomization, dosing timeline, blood collection points, frailty assessments, and downstream omics analyses. Male and female 18-month-old C57BL/6J mice were treated with 500mg/kg/day SRN-901, 300mg/kg/day NMN, or NR, Rapamycin, or placebo by oral gavage (water), and mouse cohorts were followed until the predetermined humane endpoint to determine lifespan. Mice were evaluated for frailty at 14 days before dosing (D-14; pre-dosing) and 128 days after baseline dose (D128; post-dosing). Blood samples were collected for transcriptomic and metabolomic analyses at D-7 (pre-dosing) and D56 (post-dosing). SRN-901 and Control: n= 44 per group; Rapamycin, NMN, and NR: n= 24 per group.

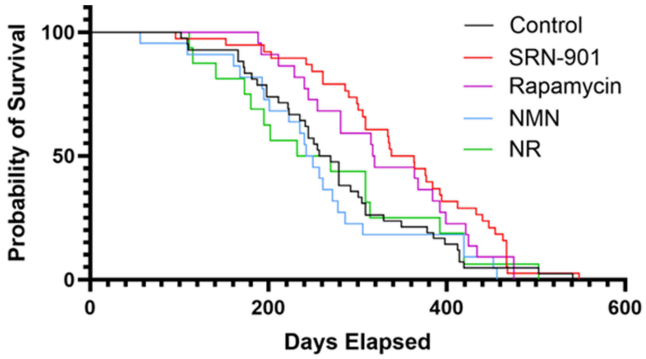

Figure 2 SRN-901 significantly increases lifespan of adult mice. Kaplan–Meier survival curves for mice treated with placebo (control, black), SRN-901 (red), rapamycin (magenta), nicotinamide mononucleotide (NMN, blue), and nicotinamide riboside (NR, green). Gehan–Breslow test: SRN-901 vs placebo, $p < 0.001$; rapamycin vs placebo, $p = 0.04$; NMN vs placebo, $p = 0.50$; NR vs placebo, $p = 0.83$. Median survival: Placebo = 263.5 days (95% CI: 241.0–305.0, n = 42), SRN-901 = 350.5 days (95% CI: 309.0–412.0, n = 38), Rapamycin = 318.0 days (95% CI: 281.0–399.0, n = 20), NMN = 246.0 days (95% CI: 195.0–278.0, n = 22), NR = 232.0 days (95% CI: 173.0–314.0, n = 16). Cox proportional hazards analysis for SRN-901 vs placebo: HR = 0.54 (95% CI: 0.34–0.85).

a hazard ratio of 0.54 (95% CI: 0.34–0.85; $p < 0.01$), indicating that SRN-901 treatment was associated with a 46% reduction in the hazard of death. While rapamycin increased lifespan in adult mice (318.0 days; 95% CI: 281.0–399.0; n = 20; $p = 0.04$), nicotinamide mononucleotide (NMN; 246.0 days; 95% CI: 195.0–278.0; n = 22; $p = 0.50$), and nicotinamide riboside (NR; 232.0 days; 95% CI: 173.0–314.0; n = 16; $p = 0.83$) did not show significant differences in median lifespan compared to placebo.

SRN-901 Administration in Adult Mice Improves Healthspan

At 64 weeks post-treatment onset, placebo-treated mice were ungroomed and displayed several end-of-life signs, including kyphosis (Figure 3A and B). In contrast, SRN-901-treated mice were well-groomed and maintained normal posture (Figure 3C and D).

https://doi.org/10.2147/DDDT.S594895

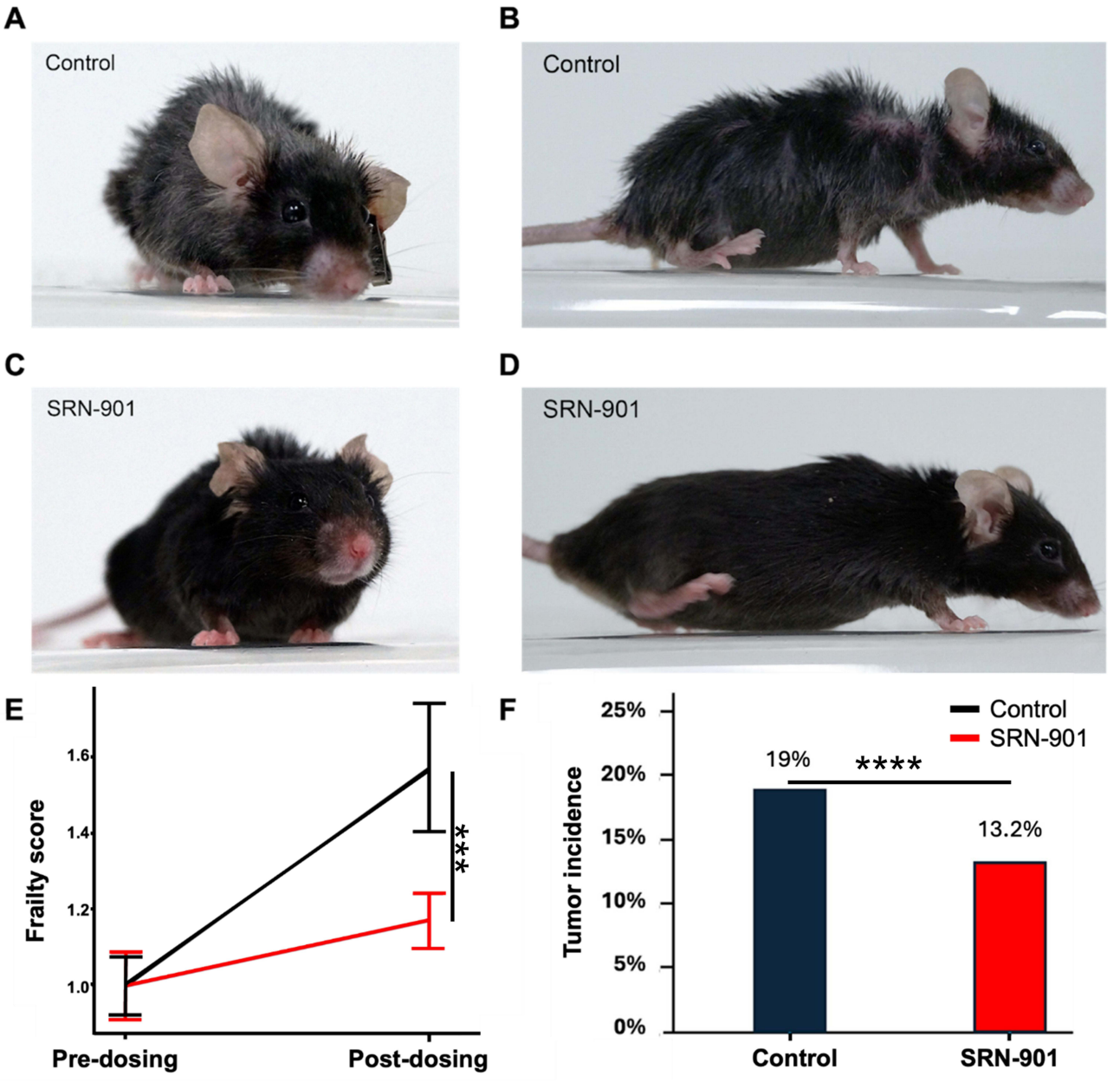

Figure 3 SRN-901 protects against frailty during aging in adult mice. (**A**–**D**) Visual inspection of mice. The photos show the mice 64 weeks after the start of placebo (**A** and **B**) and SRN-901 (**C** and **D**) treatment. (**E**) Frailty scores. All mice from control (black) and SRN-treated (red) at pre-dosing and post-dosing. Visual phenotypes shown in (**A**–**D**) (coat condition and kyphosis) were also scored using the same frailty index subscores and are reflected in the composite frailty values. (**F**) Tumor incidence rate. Adult mice from control (black) and SRN-901-treated (red) groups. Placebo: n = 42; SRN-901; n = 38. ***p<0.001, ****p<0.0001.

To further investigate the effect of SRN-901 on mouse healthspan, we performed frailty tests on all mouse cohorts at pre- and post-dosing time points. SRN-901-treated mice had a mean frailty score of 3.29 ± 1.30 at baseline and 3.85 ± 1.04 after 128 days of treatment. Whereas placebo-treated mice progressed from 2.80 ± 0.95 to 4.40 ± 2.10 over the same interval. When scores were normalized to each cohort's own baseline (set to 1.0), the placebo group increased to 1.57 while the SRN-901 group rose only to 1.17. This corresponds to a 70% attenuation of frailty progression relative to placebo controls ($p = 0.001$; Figure 3E and Supplementary Table 2.1).

Mice were also examined post-mortem for tumor growth (Figure 3F). Tumor incidence in SRN-901-treated mice (13.2%) was significantly reduced by 30.53% relative to placebo-treated mice (19.0%; $p < 0.0001$).

SRN-901 Suppresses Aging-Related Disease Pathways While Activating Transcriptional Pathways Linked to Longevity in Adult Mice

To investigate the mechanisms by which SRN-901 increases lifespan, we performed RNA sequencing (RNA-seq) to examine gene expression profiles of blood samples from SRN-901-treated and placebo-treated mice at 7 days before treatment and 56 days after the start of treatment. We identified a total of 1710 genes that were differentially regulated in SRN-901-treated mice and 1034 genes that were differentially regulated in placebo-treated mice. Of these, 1426 were unique to SRN-901-treated mice, 750 were unique to placebo-treated mice, and 284 were differentially regulated in both conditions.

Gene-set enrichment analysis (GSEA) of placebo- versus SRN-901-treated mice identified 49 differentially regulated pathways (5 upregulated; 44 downregulated) (Supplementary Table 3.1). Pathways related to DNA repair were upregulated in the SRN-901 treated mice, whereas pathways related to apoptosis, PI3K/AKT/mTOR signaling, unfolded protein response, interferon-α and -γ responses, IL6/JAK/STAT3 signaling, inflammatory response, reactive oxygen species pathway, and mTORC1 signaling were all downregulated (Figure 4A).

To investigate the effect of SRN-901 on transcriptional programs related to aging-associated diseases, we performed pathway analysis with the KEGG and KEGG disease pathway databases, comparing SRN-901-treated mice to controls. This analysis identified 214 differentially regulated pathways (159 upregulated; 55 downregulated) (Supplementary Table 3.2 and Figure 4B), including upregulation of mitophagy and autophagy pathways and downregulation of mTOR, insulin resistance, and NF-κB pathways.

KEGG Disease pathway enrichment analysis further revealed significant modulation of age-associated disease programs in SRN-901–treated mice (Figure 4C). Notably, the Alzheimer disease pathway was the most significantly enriched disease annotation and was directionally downregulated relative to placebo controls. This enrichment reflects coordinated suppression of molecular processes shared between aging and neurodegeneration, including inflammatory signaling (eg., NF-κB and JAK–STAT pathways), metabolic reprogramming (glycolysis/gluconeogenesis and cholesterol metabolism), and vesicular trafficking pathways (SNARE interactions). Because these analyses were performed on whole-blood transcriptomes, the Alzheimer's disease annotation should be interpreted as pathway-level overlap with neurodegeneration-associated molecular programs rather than evidence of disease modification or cognitive benefit.

SRN-901 Treatment in Adult Mice Inhibits Metabolic Aging

To further characterize the mechanisms underlying SRN-901-mediated lifespan extension, we performed metabolomic sequencing to examine the metabolite profiles of whole blood samples from SRN-901-treated and placebo-treated mice at 7 days before treatment and 56 days after treatment onset.

To investigate metabolic shifts in control animals from pre-dosing to post-dosing that were not reflected in the treatment group, we examined the metabolites that were naturally affected by aging. Metabolite changes observed in aging controls were blunted or reversed in SRN-901-treated mice, including 78 metabolites that were rescued by SRN-901 treatment (Supplementary Table 4.1), indicating that treatment was associated with partial normalization of age-related metabolic shifts (Figure 5A and Supplementary Table 4.2).

To gain further understanding on the pathways related to these metabolites, we utilized KEGG pathway enrichment analysis to assess the global transcriptional and metabolic shifts induced by treatment and found 25 KEGG pathways that were significantly altered (23 upregulated and 2 downregulated) (Figure 5B). Among the most significantly upregulated pathways were glutathione metabolism, insulin signaling, AMPK signaling, and FoxO signaling, all of which are well-established regulators of aging and longevity. In contrast, pathways associated with chronic inflammation, cellular senescence, and metabolic dysfunction were significantly downregulated following SRN-901 administration. An analysis of these metabolites for involvement in liver function identified the upregulation of niacinamide, phloretin, riboflavin, and S-glutathionyl-L-cysteine (Figure 5C–F) and downregulation of 11beta-PGE2, urobilin, CerP(d18_1_18_0), and glycinamide ribonucleotide (Figure 5G–J).

There was considerable overlap between the metabolomics and transcriptomics data in that, consistent with previous findings in transcriptomics, we observed significant modulation of pathways associated with longevity regulation,

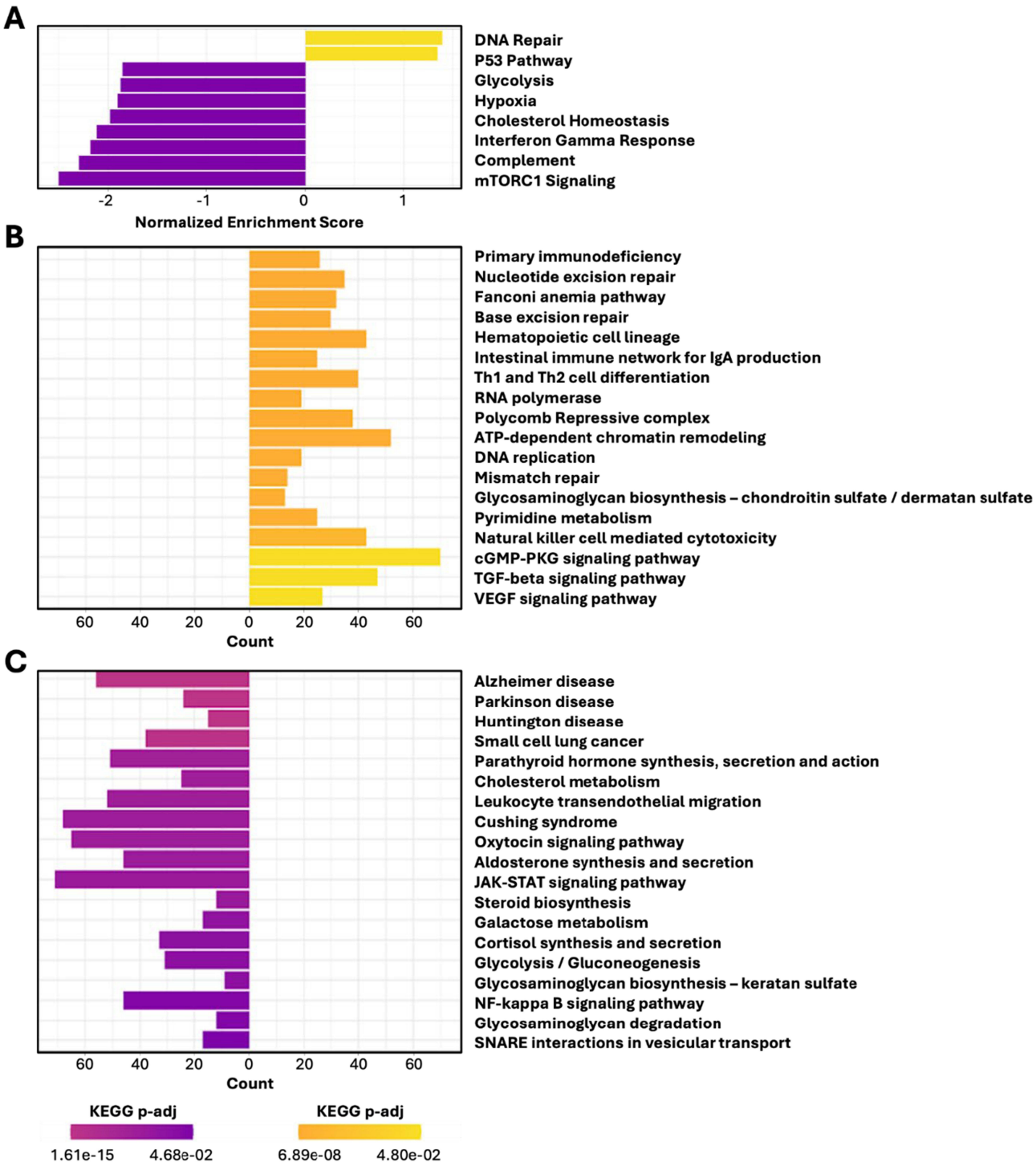

Figure 4 SRN-901 transcriptionally upregulates pro-longevity pathways and downregulates aging and aging-related disease pathways in adult mice. RNA-seq data from SRN-901 and placebo-treated mice 56 days into the daily dosing regimen were analyzed for GSEA Hallmark pathways (**A**) and KEGG pathways (**B** and **C**). n = 24 per group.

metabolic homeostasis, and age-related disease suppression. Notably, pathways central to cellular repair, energy metabolism, and stress resistance were upregulated, while pro-inflammatory and disease-associated pathways were suppressed (Figures 4A, B and 5B).

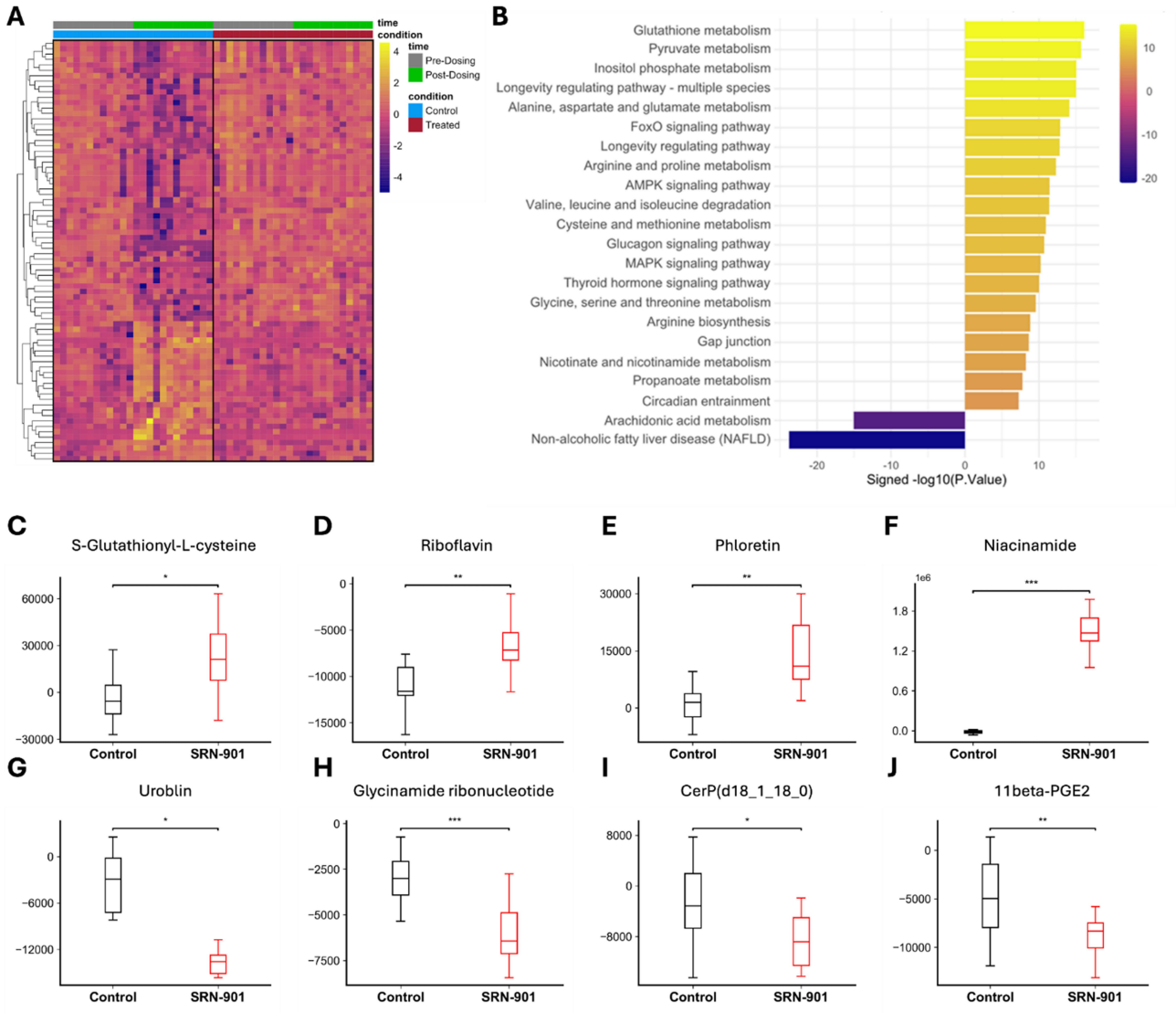

Figure 5 SRN-901 preserves the metabolic aging profile of adult mice. (**A**) Differential metabolite analysis. Metabolomics data was analyzed for metabolite levels that changed in placebo-treated mice between pre-dosing (D-7) and post-dosing (D56) and did not change between SRN-901-treated mice pre- and post-treatment, yielding metabolites rescued by SRN-901 treatment during mouse aging. (**B**) Metabolomic pathway analysis. Metabolomics data from SRN-901 and placebo-treated mice 56 days into the daily dosing regimen were analyzed with KEGG Pathway Enrichment Analysis. (**C–J**) Liver function related metabolites. Differential analysis of individual metabolites revealed an upregulation of S-Glutathionyl-L-cysteine, Riboflavin, Phloretin, and Niacinamide (**C–F**) and a downregulation of Urobilin, Glycinamide ribonucleotide, CerP (d18_1_18_0), and 11beta-PGE2 (**G–J**). n = 12 per group. *p<0.05, **p<0.01, ***p<0.001.

SRN-901 Treatment in Adult Mice Alters the Proteome

In the comprehensive proteomic profiling of the blood samples, 100,652 peptides corresponding to 10,052 protein groups were profiled across the samples and 87,174 peptides and 5023 proteins were available for statistical analysis.

To determine specific differences in protein levels between placebo- and SRN-901-treated samples overall, we performed a differential expression analysis (one-way ANOVA). Of the evaluated proteins, 47 proteins showed a statistically significant change (p adj < 0.05, log2(fc) > 1) (Figure 6A). Several of the upregulated proteins, including AADAT, PYGM, LIPA3, and KAD2, are functionally linked to amino acid metabolism, glycogen metabolism, lipid processing, and adenylate energy buffering, respectively. Conversely, downregulated proteins such as KI67, RBBP5, and PSMD5 are associated with cellular proliferation, chromatin remodeling, and proteostasis regulation. While these individual protein changes suggest functional stratification between metabolic and growth-associated processes,

https://doi.org/10.2147/DDDT.S594895

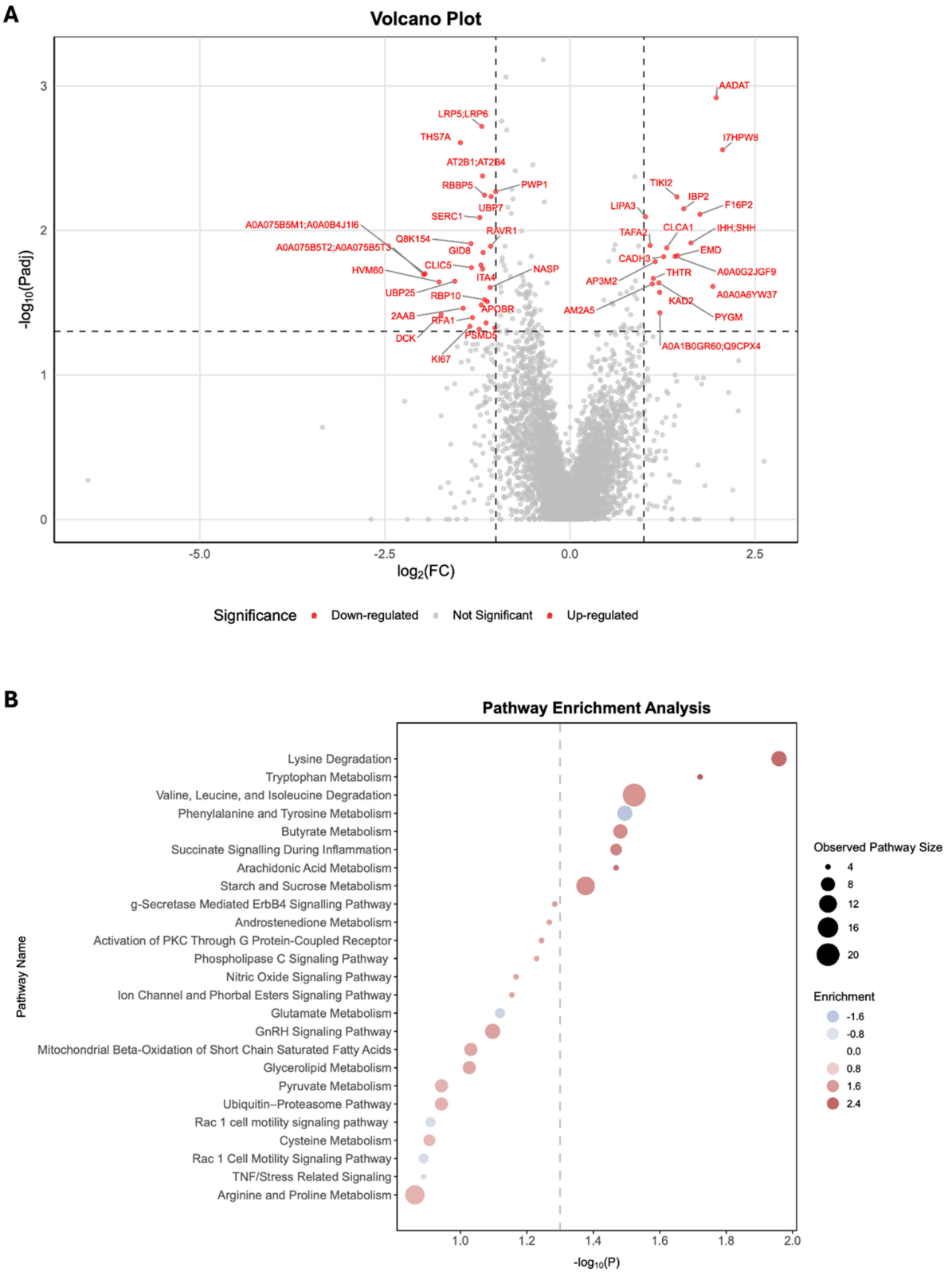

Figure 6 SRN-901 alters proteome of adult mice during aging. (**A**) Volcano plot of proteins. The adjusted p-values and $\log_2$ fold-changes of the protein abundance changes relative to the vehicle samples are plotted against each other in the plot below. Red dots indicate proteins that pass the padj < 0.05 and |log2(fc)| > 1 cutoff. (**B**) Pathway analysis. The dot plot displays the enriched pathways identified in the analysis, with their corresponding significance levels represented on the x-axis. The significance threshold (p = 0.05) is denoted by the gray dashed line. Dot size reflects the number of proteins measured in each pathway. Additionally, the color of the dots represents the enrichment, which indicates the extent to which the metabolites in the pathway were clustered amongst the compounds with the most positive fold-changes (positive enrichments), the most negative fold-changes (negative enrichments), or uniformly distributed across high and low fold-change compounds (enrichment values near 0.0). n = 24 per group.

https://doi.org/10.2147/DDDT.S594895

enrichment analysis was necessary to determine whether these alterations reflected coordinated pathway-level remodeling rather than isolated protein shifts.

To gain biological insights from the dysregulated proteins, a GSEA-based pathway analysis was conducted. The analysis identified key biochemical pathways (signaling, metabolic, and protein) that were altered between sample groups. This analysis identified eight pathways that were enriched (Figure 6B). These pathways include the upregulation of tryptophan metabolism, lysine degradation, arachidonic acid metabolism, succinate signaling during inflammation, butyrate metabolism, starch and sucrose metabolism, and valine, leucine, and isoleucine degradation in SRN-901-treated mice samples. The phenylalanine and tyrosine metabolism pathway was downregulated in SRN-901-treated mice samples.

Discussion

Our findings demonstrate that SRN-901 administration significantly increases the lifespan of mice, reduces frailty scores, modulates proteomic and gene expression pathways linked to longevity and aging-related diseases, and inhibits metabolic aging. Taken together, these results provide evidence that SRN-901 exerts its pro-longevity effects by simultaneously targeting multiple aging pathways, reinforcing the rationale for combinatorial therapeutic approaches in aging research. The observed transcriptional, proteomic, and metabolic shifts underscore SRN-901's role in promoting cellular resilience, reducing frailty, and suppressing key drivers of aging-related diseases. The results of this study highlight the potential of SRN-901 as a multi-target combinatorial approach to promote healthy aging and extend lifespan by targeting multiple aging pathways.

The molecular architecture of SRN-901 provides a coherent mechanistic framework for this systems-level effect. Nicotinamide riboside increases intracellular NAD^+ availability, thereby influencing sirtuin-dependent transcriptional regulation and mitochondrial bioenergetics. Urolithin A promotes mitophagy and mitochondrial quality control, reinforcing organelle turnover pathways intersecting with AMPK and mTOR signaling. Quercetin modulates pro-survival and inflammatory pathways, including PI3K/AKT and NF-κB–linked signaling nodes implicated in cellular stress adaptation. Alpha-lipoic acid engages AMPK-dependent metabolic control and redox regulation. In aggregate, these components converge on interconnected nutrient-sensing, mitochondrial surveillance, and stress-response networks that are repeatedly implicated across multiple hallmarks of aging. This convergence provides a mechanistic basis for the observed lifespan extension, frailty attenuation, and normalization of age-associated molecular drift.

Increased Lifespan and Healthspan

The 33% increase in median lifespan following SRN-901-treated mice represents a notable improvement over placebo-treated controls. The robust longevity benefits suggest that SRN-901 is effective as a late-life intervention, a critical factor given the limited efficacy of many anti-aging therapies when initiated in later life stages.[51] Additionally, SRN-901 provided a significant increase in lifespan extension compared to well-studied single molecule geroprotectors NMN and NR.

Rapamycin, NMN, and NR were selected as comparator controls due to their well-established roles as benchmark interventions in aging and longevity research.[52–55] Rapamycin, an mTOR inhibitor, is widely recognized for its robust lifespan-extending effects across multiple model organisms, serving as a reference standard for targeting nutrient-sensing pathways. NMN and NR, as NAD+ precursors, were chosen for their documented ability to enhance mitochondrial function, improve metabolic health, and mitigate age-associated physiological decline. By including these agents, we aimed to position SRN-901's multi-modal mechanism—combining PI3K/Akt/mTOR inhibition, autophagy activation, anti-inflammatory action, and NAD+ replenishment—within the context of current leading pharmacological strategies for promoting healthy aging and longevity.

The benchmark controls in our experiments were consistent with previously reported research on lifespan extension in mice. Research by Harrison et al demonstrated that, based on age at 90% mortality, mice fed rapamycin beginning at 600 days of age (19.7 months) led to an increase of 14% for females and 9% for males. NMN and NR, as NAD+ precursors, were chosen for their documented ability to enhance mitochondrial function, improve metabolic health, and mitigate age-associated physiological decline. Kane et al, demonstrated NMN treatment of mice beginning at 13 months increased

median lifespan by 8.5% in females, possibly due to sex-specific effects of NMN on NAD + metabolism. Zhang et al demonstrated that NR treatment of 22 to 24 months old mice for 6 weeks slightly increased lifespan (chow diet: mean 829 ± 12.0 days; NR treatment: mean 868 ± 12.4 days; $p = 0.034$).[55]

Frailty is a key indicator of healthspan, reflecting an organism's vulnerability to stressors.[56] SRN-901-treated mice exhibited a significant mitigation in frailty progression when compared to controls, indicative of improved physiological resilience. This reduction in frailty aligns with the observed improvements in lifespan, reinforcing the notion that SRN-901 not only extends life but also enhances quality of life (healthspan) in aging mice. Future studies should investigate specific frailty domains, such as physical performance, cognitive function, and immune robustness, to delineate the comprehensive health benefits of SRN-901.

Mechanistic Insights: Transcriptomics

Our study reveals that SRN-901 treatment induces a complex pattern of pathway modulation, affecting several key hallmarks of aging. Notably, we observed the downregulation of multiple pathways associated with inflammation, metabolism, and cellular homeostasis.

The downregulation of the NF-κB signaling pathway, a central regulator of inflammation and immune responses, is a common feature of anti-aging interventions. Chronic inflammation and inflammaging are major drivers of age-related decline,[57,58] and the observed downregulation likely contributes to a reduction in these harmful processes. Similarly, the decreased activation of the interferon-γ response and the complement system, also involved in immune function and inflammation, supports the notion that SRN-901 exerts a potent anti-inflammatory effect.

Furthermore, we found a downregulation of glycolysis, a central pathway for glucose metabolism. This suggests a potential shift in energy metabolism to oxidative phosphorylation, which has been found to decrease during aging, and a decrease in damaging metabolic byproducts, such as ROS.[59] Consistent with this, the downregulation of mTORC signaling, a key regulator of cell growth and metabolism, is also noteworthy. mTORC activation is associated with aging, and its inhibition is frequently observed in lifespan-extending interventions. Proteomic pathway data align with these findings, showing increased catabolism of lysine and branched-chain amino acids and elevated butyrate metabolism (see Proteomics).

SRN-901 appears to modulate cellular homeostasis at multiple levels. The downregulation of SNARE interactions in vesicular transport suggests alterations in cellular trafficking, potentially reducing the secretion of harmful substances or optimizing nutrient delivery, counteracting the dysregulation of protein trafficking seen in aging. Downregulation of pathways related to glycosaminoglycan degradation points to reduced breakdown of these molecules in the extracellular matrix, potentially preserving tissue structure and mitigating age-related inflammation. Moreover, the downregulation of cholesterol homeostasis suggests a beneficial impact on lipid metabolism, possibly reducing the risk of atherosclerosis.

In contrast to these downregulated pathways, we observed a significant upregulation of DNA repair. Accumulation of DNA damage is a critical factor in aging, and enhanced DNA repair capacity is a hallmark of interventions that extend lifespan and healthspan. The upregulation of the p53 pathway, a critical tumor suppressor that responds to cellular stress and DNA damage, likely reflects a beneficial activation of its tumor-suppressive functions. These findings are validated by the reduction in overall postmortem tumor incidence.

Recent advances in the field of senotherapeutics have highlighted the importance of tissue-specific and repurposed strategies for targeting cardiac and systemic senescence. Several cardiovascular-directed senotherapeutic approaches, including cardiac glycosides, metformin, acarbose, and other repurposed agents, have demonstrated the capacity to modulate senescent cell burden and cardiac aging phenotypes.[60,61] These studies emphasize that age-related cardiovascular decline can be influenced by compounds originally developed for unrelated indications, reinforcing the translational potential of multi-modal interventions. While SRN-901 was not designed as a tissue-specific senotherapeutic, the observed downregulation of inflammatory and mTOR-related pathways, combined with metabolic normalization, suggests mechanistic overlap with emerging cardioprotective senotherapeutic strategies.

In summary, the pattern of pathway modulation suggests that SRN-901 targets fundamental aging processes, including inflammation, metabolic dysregulation, and genomic instability. The combined effect of reducing pro-aging

pathways while enhancing protective mechanisms like DNA repair may contribute to its lifespan-extending and healthspan-promoting effects.

Metabolic Aging and Pathway Modulation

A relatively small subset of proteins (47 of 5023 tested) met our conservative significance criteria (≤50% missingness; CV <30%; MS/MS ≥2; RSD ≤25%; top 95% IQR retained; FDR <0.05). This likely reflects both biological and analytical constraints: late-life interventions can produce focused rather than global proteomic remodeling, and our requirement for an adjusted p value less than 0.05 and an absolute log2 fold change greater than one preferentially selects large-effect changes. Less pronounced but potentially biologically relevant shifts may therefore fall below our detection threshold and should be explored in future targeted studies.

AADAT is involved in the metabolism of tryptophan and α-aminoadipic acid and participates in several amino acid and neurotransmitter-related pathways, suggesting a potential link to metabolic and neuromodulatory processes. However, our data do not establish a causal role for AADAT in the lifespan extension observed with SRN-901, and functional studies will be required to determine whether AADAT upregulation contributes directly to the pro-longevity phenotype.

The pathways that were notably upregulated include glutathione metabolism, insulin signaling, AMPK signaling, and FoxO signaling, all of which are recognized regulators of aging and longevity. Glutathione metabolism plays a pivotal role in antioxidant defense by mitigating oxidative stress, which is a primary driver of cellular damage and dysfunction in aging tissues.[62] Similarly, activation of the AMPK and insulin signaling pathways is associated with improved metabolic flexibility, enhanced autophagy, and increased lifespan in multiple model organisms.[63–65] The upregulation of FoxO signaling further supports the hypothesis that SRN-901 enhances stress resistance, as FoxO transcription factors are key mediators of longevity-promoting interventions such as caloric restriction and exercise.[66]

Conversely, pathways linked to chronic inflammation, cellular senescence, and metabolic dysfunction were markedly downregulated after the administration of SRN-901. Suppression of arachidonic acid metabolism suggests a reduction in pro-inflammatory eicosanoid production, aligning with previous transcriptomic findings that demonstrated a decrease in IL6/JAK/STAT3 and interferon signaling. Additionally, downregulation of the non-alcoholic fatty liver disease (NAFLD) pathway indicates that SRN-901 protects against metabolic aging, preserving hepatic function and reducing lipid accumulation in aging tissues. These findings are consistent with the observed maintenance of a youthful metabolic profile in treated mice and highlight SRN-901's potential to mitigate aging-associated metabolic disorders. This metabolic preservation likely contributes to the observed lifespan extension and reduced frailty.

The observed upregulation and downregulation of specific metabolites following SRN-901 treatment provide critical insights into its mechanisms for improving lifespan and healthspan. Among the upregulated metabolites, niacinamide (a form of vitamin B3) is a key precursor in NAD+ biosynthesis, supporting cellular energy metabolism and DNA repair, processes essential for maintaining cellular function and delaying aging.[67] Phloretin, a polyphenolic compound, is known for its antioxidant and anti-inflammatory properties, potentially reducing oxidative damage and chronic inflammation associated with aging.[68] Riboflavin (vitamin B2) plays a pivotal role in mitochondrial energy production and redox balance, which are often compromised with age.[69] Deoxycholic acid, a secondary bile acid, may contribute to improved gut microbiota composition and metabolic health.[70,71] Dihydropteroate, a precursor in folate biosynthesis, underscores the importance of folate metabolism in DNA synthesis and repair.[72] S-Glutathionyl-L-cysteine, involved in redox homeostasis, reflects enhanced antioxidant defenses and mitigating oxidative stress, a hallmark of aging.[73]

Conversely, the downregulation of metabolites like 11β-prostaglandin E2 (11β-PGE2), linked to chronic inflammation, suggests reduced inflammatory signaling, which is critical for mitigating inflammaging.[74] CerP(d18:1/18:0), a ceramide phosphate, is associated with pro-inflammatory and apoptotic signaling, so its suppression may promote cell survival.[75,76] Lastly, decreased glycinamide ribonucleotide levels, a purine biosynthesis intermediate, could reflect reduced metabolic stress.

Together, these metabolic shifts reveal that SRN-901 promotes a systemic recalibration of metabolic pathways favoring enhanced mitochondrial function, reduced inflammation, and improved cellular resilience, collectively contributing to prolonged lifespan and healthspan.

Limitations and Future Directions

While this study provides compelling evidence for the efficacy of SRN-901 in promoting healthy aging, several limitations and next steps should be considered. Regarding dose schedule and optimization, we used a single total daily dose and dosing schedule. Future studies should perform dose-ranging (including lower total doses) and schedule optimization (eg, 3 days/week vs 6 days/week, and intermittent vs continuous dosing) to determine the minimal effective exposure for survival and frailty outcomes while improving translational feasibility and tolerability. Pharmacokinetic and exposure confirmation studies should be paired with pharmacodynamic readouts that reflect pathway engagement, such as NAD-related metabolites, redox markers, and inflammatory mediators.

For generalizability, the current work was performed in C57BL/6 mice under a Western diet paradigm. Validation in additional aging contexts is needed, including standard chow aging, genetically diverse strains, and disease-enriched models relevant to late-life mortality such as diet-induced metabolic dysfunction, atherosclerosis-prone backgrounds, or models of neurodegenerative decline. These studies would clarify how diet and baseline disease burden influence effect size and mechanism.

Regarding individual component contributions, SRN-901 is a combinatorial investigational longevity drug, and it will be important to quantify the contribution of each component. Future work should include factorial or ablation designs that test single agents and defined sub-combinations, with pathway engagement readouts matched to each component's expected biology.

Finally, future studies should pre-specify molecular biomarkers that are hypothesized to track with functional decline and survival, then test whether those biomarkers predict frailty trajectories, specific frailty domains (mobility, endurance, cognition, immune resilience), and mortality risk within and across cohorts. In parallel, more comprehensive pathology and organ-level functional testing, including systematic histopathology and clinical chemistry, will strengthen interpretation of cause-of-death patterns and help distinguish disease modification from generalized stress resistance.

Conclusion

This study establishes SRN-901 as a promising candidate for promoting longevity and functional healthspan, as evidenced by delayed frailty progression and reduced mortality risk in late-life treated mice. The multi-target combinatorial nature of SRN-901, designed to target multiple aging pathways simultaneously, represents a significant advancement over single-compound interventions. By addressing the interconnected and dynamic nature of aging processes, SRN-901 exemplifies the potential of combinatorial approaches to develop effective anti-aging interventions. Although the number of significantly altered proteins was modest relative to the total proteome, the changes were enriched within biologically coherent pathways relevant to aging biology. The multi-omics findings—highlighting modulation of nutrient-sensing, inflammatory, DNA repair, and metabolic stress-response pathways—provide a mechanistic framework linking these molecular shifts to the observed attenuation of frailty progression and reduction in mortality risk. The success of SRN-901 underscores the potential for combination therapies to achieve convergent pathway engagement, consistent with additive or potentially synergistic mechanisms that are required to address the inherent complexity of aging processes.

These observations underscore the multifaceted efficacy of SRN-901 and its potential translational relevance to human aging and age-related diseases. The translational implications of these findings are significant, paving the way for future research aimed at improving human healthspan and reducing the burden of age-related diseases. Future work should compare SRN-901 with emerging agents, as well as repurposed cardiometabolic drugs with senotherapeutic properties. The integration of combinatorial, tissue-directed, and repurposed approaches may enable more precise targeting of age-associated pathologies and should be considered in future combination therapy designs. Additionally, future studies should aim to delineate the contribution of individual components within SRN-901 to these pathway alterations and explore SRN-901's potential for translation into human aging interventions.

Funding

This study was funded by Seragon.

Disclosure

All authors except Jiaqi Chen and Yongzheng Liu are employees/shareholders of Seragon, which developed the investigational compound. The authors report no other conflicts of interest in this work.

References

1. Garmany A, Yamada S, Terzic A. Longevity leap: mind the healthspan gap. *NPJ Regen Med*. 2021;6(1):57. doi:10.1038/s41536-021-00169-5
2. Guo J, Huang X, Dou L, et al. Aging and aging-related diseases: from molecular mechanisms to interventions and treatments. *Signal Transduct Target Ther*. 2022;7(1):391. doi:10.1038/s41392-022-01251-0
3. Liu JK. Antiaging agents: safe interventions to slow aging and healthy life span extension. *Nat Prod Bioprospect*. 2022;12(1):18. doi:10.1007/s13659-022-00339-y
4. Barardo D, Thornton D, Thoppil H, et al. The DrugAge database of aging-related drugs. *Aging Cell*. 2017;16(3):594–597. doi:10.1111/acel.12585
5. Tacutu R, Thornton D, Johnson E, et al. Human ageing genomic resources: new and updated databases. *Nucleic Acids Res*. 2018;46(D1):D1083–D1090. doi:10.1093/nar/gkx1042
6. Mao R, Li J, Xiao W. Identification of prospective aging drug targets via Mendelian randomization analysis. *Aging Cell*. 2024;23(7):e14171. doi:10.1111/acel.14171
7. Rybina OY, Symonenko AV, Pasyukova EG. Compound combinations targeting longevity: challenges and perspectives. *Ageing Res Rev*. 2023;85:101851. doi:10.1016/j.arr.2023.101851
8. Du N, Yang R, Jiang S, et al. Anti-aging drugs and the related signal pathways. *Biomedicines*. 2024;12(1):127. doi:10.3390/biomedicines12010127
9. Center for Drug Evaluation and Research. S5(R3) detection of reproductive and developmental toxicity for human pharmaceuticals. 2021. Available from: https://www.fda.gov/regulatory-information/search-fda-guidance-documents/s5r3-detection-reproductive-and-developmental-toxicity-human-pharmaceuticals. Accessed December 24, 2025.
10. Handelsman Y, Butler J, Bakris GL, et al. Early intervention and intensive management of patients with diabetes, cardiorenal, and metabolic diseases. *J Diabetes Complications*. 2023;37(2):108389. doi:10.1016/j.jdiacomp.2022.108389
11. Tian Y, Yi J, Wang N, et al. DDInter 2.0: an enhanced drug interaction resource with expanded data coverage, new interaction types, and improved user interface. *Nucleic Acids Res*. 2025;53(D1):D1356–D1362. doi:10.1093/nar/gkae726
12. Panchin AY, Ogmen A, Blagodatski AS, Egorova A, Batin M, Glinin T. Targeting multiple hallmarks of mammalian aging with combinations of interventions. *Aging*. 2024;16(16):12073–12100. doi:10.18632/aging.206078
13. Dutta S, Sengupta P. Men and mice: relating their ages. *Life Sci*. 2016;152:244–248. doi:10.1016/j.lfs.2015.10.025
14. Whitehead JC, Hildebrand BA, Sun M, et al. A clinical frailty index in aging mice: comparisons with frailty index data in humans. *J Gerontol Ser A*. 2014;69(6):621–632. doi:10.1093/gerona/glt136
15. Chen S, Zhou Y, Chen Y, Gu J. fastp: an ultra-fast all-in-one FASTQ preprocessor. *Bioinformatics*. 2018;34(17):i884–i890. doi:10.1093/bioinformatics/bty560
16. Chen S. Ultrafast one-pass FASTQ data preprocessing, quality control, and deduplication using fastp. *Imeta*. 2023;2(2):e107. doi:10.1002/imt2.107
17. Deng ZL, Münch PC, Mreches R, McHardy AC. Rapid and accurate identification of ribosomal RNA sequences via deep learning. *Nucleic Acids Res*. 2022;50(10):e60. doi:10.1093/nar/gkac112
18. Dobin A, Davis CA, Schlesinger F, et al. STAR: ultrafast universal RNA-seq aligner. *Bioinformatics*. 2013;29(1):15–21. doi:10.1093/bioinformatics/bts635
19. Li H, Handsaker B, Wysoker A, et al. The sequence alignment/map format and SAMtools. *Bioinformatics*. 2009;25(16):2078–2079. doi:10.1093/bioinformatics/btp352
20. Liao Y, Smyth GK, Shi W. featureCounts: an efficient general purpose program for assigning sequence reads to genomic features. *Bioinformatics*. 2014;30(7):923–930. doi:10.1093/bioinformatics/btt656
21. Love MI, Huber W, Anders S. Moderated estimation of fold change and dispersion for RNA-seq data with DESeq2. *Genome Biol*. 2014;15(12):550. doi:10.1186/s13059-014-0550-8
22. Robinson MD, McCarthy DJ, Smyth GK. edgeR: a Bioconductor package for differential expression analysis of digital gene expression data. *Bioinformatics*. 2010;26(1):139–140. doi:10.1093/bioinformatics/btp616
23. Klipper-Aurbach Y, Wasserman M, Braunspiegel-Weintrob N, et al. Mathematical formulae for the prediction of the residual beta cell function during the first two years of disease in children and adolescents with insulin-dependent diabetes mellitus. *Med Hypotheses*. 1995;45(5):486–490. doi:10.1016/0306-9877(95)90228-7
24. de Magalhães JP, Abidi Z, Dos Santos GA, et al. Human ageing genomic resources: updates on key databases in ageing research. *Nucleic Acids Res*. 2024;52(D1):D900–D908. doi:10.1093/nar/gkad927
25. Bunu G, Toren D, Ion CF, et al. SynergyAge, a curated database for synergistic and antagonistic interactions of longevity-associated genes. *Sci Data*. 2020;7(1):366. doi:10.1038/s41597-020-00710-z
26. Aging Atlas Consortium. Aging Atlas: a multi-omics database for aging biology. *Nucleic Acids Res*. 2021;49(D1):D825–D830. doi:10.1093/nar/gkaa894
27. Wu T, Hu E, Xu S, et al. clusterProfiler 4.0: a universal enrichment tool for interpreting omics data. *Innovation*. 2021;2(3):100141. doi:10.1016/j.xinn.2021.100141
28. Supek F, Bošnjak M, Škunca N, Šmuc T. REVIGO summarizes and visualizes long lists of gene ontology terms. *PLoS One*. 2011;6(7):e21800. doi:10.1371/journal.pone.0021800
29. Reiner A, Yekutieli D, Benjamini Y. Identifying differentially expressed genes using false discovery rate controlling procedures. *Bioinformatics*. 2003;19(3):368–375. doi:10.1093/bioinformatics/btf877
30. Korotkevich G, Sukhov V, Budin N, Shpak B, Artyomov MN, Sergushichev A. Fast gene set enrichment analysis. *bioRxiv*. 2021;060012. doi:10.1101/060012
31. Liberzon A, Birger C, Thorvaldsdóttir H, Ghandi M, Mesirov JP, Tamayo P. The Molecular Signatures Database (MSigDB) hallmark gene set collection. *Cell Syst*. 2015;1(6):417–425. doi:10.1016/j.cels.2015.12.004

32. Barzilai N, Huffman DM, Muzumdar RH, Bartke A. The critical role of metabolic pathways in aging. *Diabetes*. 2012;61(6):1315–1322. doi:10.2337/db11-1300
33. Luo W, Brouwer C. Pathview: an R/Bioconductor package for pathway-based data integration and visualization. *Bioinformatics*. 2013;29(14):1830–1831. doi:10.1093/bioinformatics/btt285
34. Kessner D, Chambers M, Burke R, Agus D, Mallick P. ProteoWizard: open source software for rapid proteomics tools development. *Bioinformatics*. 2008;24(21):2534–2536. doi:10.1093/bioinformatics/btn323
35. Smith CA, Want EJ, O'Maille G, Abagyan R, Siuzdak G. XCMS: processing mass spectrometry data for metabolite profiling using nonlinear peak alignment, matching, and identification. *Anal Chem*. 2006;78(3):779–787. doi:10.1021/ac051437y
36. Wei R, Wang J, Su M, et al. Missing value imputation approach for mass spectrometry-based metabolomics data. *Sci Rep*. 2018;8(1):663. doi:10.1038/s41598-017-19120-0
37. Jian L, Shen S, Li J, Liang X, Li L. Budget online learning algorithm for least squares SVM. *IEEE Trans Neural Netw Learn Syst*. 2017;28(9):2076–2087. doi:10.1109/TNNLS.2016.2574332
38. Wishart DS, Guo A, Oler E, et al. HMDB 5.0: the human metabolome database for 2022. *Nucleic Acids Res*. 2022;50(D1):D622–D631. doi:10.1093/nar/gkab1062
39. Wishart DS, Tzur D, Knox C, et al. HMDB: the human metabolome database. *Nucleic Acids Res*. 2007;35(Database issue):D521–526. doi:10.1093/nar/gkl923
40. Smith CA, O'Maille G, Want EJ, et al. METLIN: a metabolite mass spectral database. *Ther Drug Monit*. 2005;27(6):747–751. doi:10.1097/01.ftd.0000179845.53213.39
41. Woolson RF. Wilcoxon signed-rank test. In: *Encyclopedia of Biostatistics*. John Wiley & Sons, Ltd; 2005. doi10.1002/0470011815.b2a15177
42. Ruxton GD. The unequal variance t-test is an underused alternative to Student's t-test and the Mann–Whitney U test. *Behav Ecol*. 2006;17(4):688–690. doi:10.1093/beheco/ark016
43. McKnight PE, Najab J. Mann–Whitney U Test. In: *The Corsini Encyclopedia of Psychology*. John Wiley & Sons, Inc; 2010. doi:10.1002/9780470479216.corpsy0524
44. Demichev V, Messner CB, Vernardis SI, Lilley KS, Ralser M. DIA-NN: neural networks and interference correction enable deep proteome coverage in high throughput. *Nat Methods*. 2020;17(1):41–44. doi:10.1038/s41592-019-0638-x
45. Cox J, Hein MY, Luber CA, Paron I, Nagaraj N, Mann M. Accurate proteome-wide label-free quantification by delayed normalization and maximal peptide ratio extraction, termed MaxLFQ. *Mol Cell Proteomics*. 2014;13(9):2513–2526. doi:10.1074/mcp.M113.031591
46. Leek JT, Johnson WE, Parker HS, Jaffe AE, Storey JD. The sva package for removing batch effects and other unwanted variation in high-throughput experiments. *Bioinformatics*. 2012;28(6):882–883. doi:10.1093/bioinformatics/bts034
47. Girden ER. *ANOVA*. SAGE Publications, Inc.; 1992. doi:10.4135/9781412983419
48. Ritchie ME, Phipson B, Wu D, et al. limma powers differential expression analyses for RNA-sequencing and microarray studies. *Nucleic Acids Res*. 2015;43(7):e47. doi:10.1093/nar/gkv007
49. Wishart AL, Conner SJ, Guarin JR, et al. Decellularized extracellular matrix scaffolds identify full-length collagen VI as a driver of breast cancer cell invasion in obesity and metastasis. *Sci Adv*. 2020;6(43):eabc3175. doi:10.1126/sciadv.abc3175
50. Thomas PD, Hill DP, Mi H, et al. Gene Ontology Causal Activity Modeling (GO-CAM) moves beyond GO annotations to structured descriptions of biological functions and systems. *Nat Genet*. 2019;51(10):1429–1433. doi:10.1038/s41588-019-0500-1
51. Chaudhari PS, Ermolaeva MA. Too old for healthy aging? Exploring age limits of longevity treatments. *NPJ Metab Health Dis*. 2024;2(1):37. doi:10.1038/s44324-024-00040-3
52. Harrison DE, Strong R, Sharp ZD, et al. Rapamycin fed late in life extends lifespan in genetically heterogeneous mice. *Nature*. 2009;460(7253):392–395. doi:10.1038/nature08221
53. Mills KF, Yoshida S, Stein LR, et al. Long-term administration of nicotinamide mononucleotide mitigates age-associated physiological decline in mice. *Cell Metab*. 2016;24(6):795–806. doi:10.1016/j.cmet.2016.09.013
54. Kane A, Chellappa K, Schultz M, et al. Long-term NMN treatment increases lifespan and healthspan in mice in a sex dependent manner. *Innov Aging*. 2023;7(Suppl 1):1077. doi:10.1093/geroni/igad104.3459
55. Zhang H, Ryu D, Wu Y, et al. NAD^+ repletion improves mitochondrial and stem cell function and enhances life span in mice. *Science*. 2016;352(6292):1436–1443. doi:10.1126/science.aaf2693
56. Palliyaguru DL, Moats JM, Di Germanio C, Bernier M, de Cabo R. Frailty index as a biomarker of lifespan and healthspan: focus on pharmacological interventions. *Mech Ageing Dev*. 2019;180:42–48. doi:10.1016/j.mad.2019.03.005
57. Ferrucci L, Fabbri E. Inflammageing: chronic inflammation in ageing, cardiovascular disease, and frailty. *Nat Rev Cardiol*. 2018;15(9):505–522. doi:10.1038/s41569-018-0064-2
58. Li X, Li C, Zhang W, Wang Y, Qian P, Huang H. Inflammation and aging: signaling pathways and intervention therapies. *Signal Transduct Target Ther*. 2023;8(1):239. doi:10.1038/s41392-023-01502-8
59. Elmansi AM, Miller RA. Oxidative phosphorylation and fatty acid oxidation in slow-aging mice. *Free Radic Biol Med*. 2024;224:246–255. doi:10.1016/j.freeradbiomed.2024.08.018
60. Atasever E, Atayik MC, Çakatay U. Senotherapeutics: milestones, innovations, and future prospects. In: *Advances in Pharmacology*. Vol. 104. Academic Press; 2025:1–35. doi:10.1016/bs.apha.2025.01.021
61. Cebe T, Kızılyel F. Risk of senescence, polypharmacy, and their outcomes in elderly cardiovascular disease patients. In: *Advances in Pharmacology*. Vol. 104. Academic Press; 2025:351–392. doi:10.1016/bs.apha.2025.02.011
62. Yang J, Luo J, Tian X, Zhao Y, Li Y, Wu X. Progress in understanding oxidative stress, aging, and aging-related diseases. *Antioxidants*. 2024;13(4):394. doi:10.3390/antiox13040394
63. Steinberg GR, Carling D. AMP-activated protein kinase: the current landscape for drug development. *Nat Rev Drug Discov*. 2019;18(7):527–551. doi:10.1038/s41573-019-0019-2
64. Soo SK, Rudich ZD, Ko B, Moldakozhayev A, AlOkda A, Van Raamsdonk JM. Biological resilience and aging: activation of stress response pathways contributes to lifespan extension. *Ageing Res Rev*. 2023;88:101941. doi:10.1016/j.arr.2023.101941
65. Gómez J, Mota-Martorell N, Jové M, Pamplona R, Barja G. Mitochondrial ROS production, oxidative stress and aging within and between species: evidences and recent advances on this aging effector. *Exp Gerontol*. 2023;174:112134. doi:10.1016/j.exger.2023.112134

66. Santos BF, Grenho I, Martel PJ, Ferreira BI, Link W. FOXO family isoforms. *Cell Death Dis*. 2023;14(10):702. doi:10.1038/s41419-023-06177-1
67. Mitchell SJ, Bernier M, Aon MA, et al. Nicotinamide improves aspects of healthspan, but not lifespan, in mice. *Cell Metab*. 2018;27(3):667–676.e4. doi:10.1016/j.cmet.2018.02.001
68. Mariadoss AVA, Vinyagam R, Rajamanickam V, Sankaran V, Venkatesan S, David E. Pharmacological aspects and potential use of phloretin: a systemic review. *Mini Rev Med Chem*. 2019;19(13):1060–1067. doi:10.2174/1389557519666190311154425
69. Suwannasom N, Kao I, Pruß A, Georgieva R, Bäumler H. Riboflavin: the health benefits of a forgotten natural vitamin. *Int J Mol Sci*. 2020;21(3):950. doi:10.3390/ijms21030950
70. Larabi AB, Masson HLP, Bäumler AJ. Bile acids as modulators of gut microbiota composition and function. *Gut Microbes*. 2023;15(1):2172671. doi:10.1080/19490976.2023.2172671
71. Zhang L, Zheng Z, Huang H, et al. Multi-omics reveals deoxycholic acid modulates bile acid metabolism via the gut microbiota to antagonize carbon tetrachloride-induced chronic liver injury. *Gut Microbes*. 2024;16(1):2323236. doi:10.1080/19490976.2024.2323236
72. Duthie SJ. Folate and cancer: how DNA damage, repair and methylation impact on colon carcinogenesis. *J Inherit Metab Dis*. 2011;34(1):101–109. doi:10.1007/s10545-010-9128-0
73. Sekhar RV, Patel SG, Guthikonda AP, et al. Deficient synthesis of glutathione underlies oxidative stress in aging and can be corrected by dietary cysteine and glycine supplementation. *Am J Clin Nutr*. 2011;94(3):847–853. doi:10.3945/ajcn.110.003483
74. Srour E, Martin N, Drullion C, et al. Prostaglandin E2 regulates senescence and post-senescence neoplastic escape in primary human keratinocytes. *Aging*. 2024;16(21):13201–13224. doi:10.18632/aging.206149
75. Yu XD, Wang JW. Ceramide de novo synthesis in non-alcoholic fatty liver disease: pathogenic mechanisms and therapeutic perspectives. *Biochem Pharmacol*. 2022;202:115157. doi:10.1016/j.bcp.2022.115157
76. Alizadeh J, da Silva Rosa SC, Weng X, et al. Ceramides and ceramide synthases in cancer: focus on apoptosis and autophagy. *Eur J Cell Biol*. 2023;102(3):151337. doi:10.1016/j.ejcb.2023.151337